SYNTHESIS AND EMERGING IDEAS

Proliferating particle surface area via microbial decay has profound consequences for remineralisation rate: a new approach to modelling the degradation of sinking detritus in the ocean

Thomas R. Anderson · **Wendy C. Gentleman** ·
B. B. Cael · **Joël J.-M. Hirschi** ·
Robert L. Eastwood · **Daniel J. Mayor**

Abstract Sinking detritus particles in the ocean help to regulate global climate by transporting organic carbon into deep waters where it is sequestered from the atmosphere. The rate at which bacteria remineralise detritus influences how deep particles sink and the length-scale of carbon sequestration. Conventional marine biogeochemical models typically represent particles as smooth spheres where remineralisation causes surface area (SA) to progressively shrink over time. In contrast, we propose that particle SA increases during degradation as microbial ectoenzymes cause a roughening of surfaces in a process similar to acid etching on previously smooth glass or metal surfaces. This concept is investigated using a novel model, SAMURAI (Surface Area Modelling Using Rubik As Inspiration), in which the biomass of individual particles is represented as a 3D matrix of cubical sub-units that degrades by progressive removal of sub-units that have faces in contact with the external environment. The model rapidly generates microscale rugosity (roughness) that profoundly increases total SA, giving rise to biomass-specific remineralisation rates that are approximately double those of conventional models. Faster remineralisation means less carbon penetrates the ocean's interior, diminishing carbon sequestration in deep waters. Results indicate that both SA and microbial remineralisation are highly dynamic, as well as exhibiting large variability associated with particles of different porosities. Our work highlights the need for further studies, both observational and modelling, to investigate particle SA and related microbial dynamics in order to reliably represent the role of ocean biology in global biogeochemical models.

Keywords Ocean carbon sequestration · Remineralisation length-scale · Detritus degradation · Surface area · Particle-attached bacteria · Marine ecosystem model

T. R. Anderson (✉) · J. J.-M. Hirschi
Marine Systems Modelling, National Oceanography Centre, Southampton SO14 3ZH, UK
e-mail: tra@noc.ac.uk

W. C. Gentleman
Department of Engineering Mathematics, Dalhousie University, Halifax, NS, B3J 1B6, Canada

B. B. Cael · D. J. Mayor
Ocean Biogeosciences, National Oceanography Centre, Southampton SO14 3ZH, UK

R. L. Eastwood
1942 Rosebank Ave, Halifax, NS B3H 4C7, Canada

Present Address:
D. J. Mayor
Biosciences, Hatherly Building, University of Exeter, Exeter EX4 4PS, UK

Introduction

Photosynthesis by ocean phytoplankton generates ~ 48 Gt organic carbon (C) annually (Field et al. 1998) of which approximately 5–10% sinks to depths > 1000 m as detrital particles (Henson et al. 2012) where the constituent C remains isolated from the atmosphere for centennial to millennial timescales. This vertical flux of sinking organic matter, widely referred to as the biological gravitational pump (BGP; Boyd et al. 2019), plays a key role in regulating global climate; without it, atmospheric CO_2 would be 200 ppm higher than it is today (Kwon et al. 2009). The strength of the BGP depends on the rate at which sinking organic matter is remineralised via microbial respiration. There is, however, large variation in the predicted length-scale of C remineralisation across different ocean biogeochemical models (Henson et al. 2012; Marsay et al. 2015; Wilson et al. 2022). This variation reflects uncertainty in our knowledge of the processes that influence the fate of sinking particles in the ocean and highlights the need for improved understanding in order to reliably simulate ocean-climate interactions and how these may change throughout the twenty-first century.

Remineralisation of sinking detrital particles is carried out by heterotrophic bacteria which degrade the organic C using ectoenzymes and use it for growth and respiration (Chróst 1992; Arnosti 2011). There are two main considerations when deriving equations for this process in ocean models: representation of detrital biomass and parameterisation of its degradation by microbes. The simplest approach to the former is to represent detritus as a bulk state variable in which case degradation is described as a rate per unit biomass, as is usually the case in the global ocean models (Yool et al. 2013; Aumont et al. 2015; Kriest and Oschlies 2015). Detritus can alternatively be modelled as individual particles that are most simply represented as spheres (Vetter et el. 1998; Bianchi et al. 2018; Alcolombri et al. 2021; Nguyen et al. 2022). Degradation may then be calculated using biomass-specific rates as in the global models, or based on proportionality to SA or volume (Omand et al. 2020). The most intuitive assumption is proportionality to SA, given that ectoenzymes act on surfaces which are thereby a key factor in regulating the growth of particle-attached microbes (Enke et al. 2018). Decreasing particle biomass

during degradation means decreasing size. In turn, this leads to lower SA if particles are represented as simple geometric shapes such as smooth spheres. This trend of decreasing SA with diminishing particle size is, we propose, overly simplistic. In the real world, sinking particles are often complex shapes and, crucially, enzymatic degradation may alter a particle's shape and surface characteristics in a non-uniform manner, of which little is known.

Here, we challenge the fundamental concept that the SA of a detritus particle will progressively decrease during degradation. Instead, we propose that enzymatic degradation will generate microstructure and hence rugosity that increases a particle's SA relative to its initial condition, with profound implications for predicting C remineralisation and sequestration in the ocean. Consider a grub burrowing into an apple. The resulting tunnel greatly increases the SA exposed to the external environment whilst having only a relatively modest effect on total volume. Although the process of enzymatic hydrolysis does not correspond exactly with that of a burrowing grub, we propose that the concept is nevertheless the same in that the action of ectoenzymes will generate micro-scale rugosity, proliferating SA in a process that may be thought of as being analogous to acid etching on previously smooth glass or metal surfaces. As a consequence, the predicted remineralisation of organic C will be faster than when using conventional modelling approaches such as shrinking spheres. We investigate our idea using a novel model, SAMURAI_1.0 (Surface Area Modelling Using Rubik As Inspiration, version 1.0), in which individual detrital particles, either single or as aggregates, are represented as a 3D matrix of cubes, hereafter referred to as sub-units, structured in analogous fashion to the well-known Rubik's Cube invented by Enrö Rubik in 1974 (Demaine et al. 2011). The SAMURAI model is used to study the relationship between SA and particle volume (biomass) as degradation takes place, simulated as progressive removal of sub-units that have faces in contact with the external environment. Time-dependent C remineralisation rates are then calculated by incorporating the predicted trends in SA into a simple model of microbial consumption of detritus and these rates are compared with those calculated for particles represented as standard spheres. Model results are discussed in context of remineralisation length

scales and the associated consequences for ocean C sequestration.

The SAMURAI model

Description

A new model of microbial degradation is developed in which the volume of a single detrital particle is represented as a 3D matrix of cubical sub-units, akin to the well-known Rubik's Cube. The volume occupied by sub-units and biomass can be used interchangeably assuming that substrate density is homogeneous. The matrix has dimensions in x–y–z and is specified in terms of grid resolution (GR), e.g., a GR of 25× represents maximum dimensions (outermost edges of the object) of 25×25×25 sub-units. It can be entirely filled with sub-units from the outset, generating a solid cuboid, or can alternatively be populated to give other chosen shapes. We investigate spherical particles although also show images and results for simulations of degrading prolate spheroids (oblong pellet shapes) in Supplementary Appendix 1.

In reality, microbes use particulate organic matter for growth and metabolism only after it has been solubilised using hydrolytic ectoenzymes that act on exposed detrital surfaces (Smith et al. 1992). We simulate this process by sequential removal of sub-units (volume, mass) from the matrix based on exposed SA (in contact with the external environment). At each step in the simulation, the computer randomly selects a single exposed face from among all exposed faces within the matrix and the associated sub-unit is removed, exposing new faces associated with adjacent sub-units. The probability of a given sub-unit being removed at a given point in the simulation is thus highest if it has multiple exposed faces, where the number varies between 0 (the sub-unit is situated within the particle's interior) and 6 (the sub-unit has broken free). Note that the length of time that a sub-unit has been exposed during the simulation has no bearing on its potential selection for removal in that we assume that exposed SA is rapidly colonised by microbes from the surrounding water. Sub-unit removal continues until the matrix is left empty, at which point degradation is complete. Our approach assumes that degradation rate is constant per unit SA

and that, for practical purposes, SA removal is discrete as single sub-units in sequence.

Shape and grid resolution

For illustrative purposes, model simulations are first shown for Rubik spheres using a relatively coarse GR of 25×. The simulated degradation leads to irregular SA and increased rugosity, with small fragments cleaving off while the central core remains largely intact until the latter stages (Fig. 1A). We will also investigate aggregates made up of sub-particles and, in anticipation of those results, Fig. 1B shows the degradation of one such 50× aggregate, made up of sub-particles of 11× diameter.

The model was next run 10 times for each of seven Rubik configurations for GRs of 10×, 25×, 50×, 125×, 250×, 500× and 2000× (Fig. 2). The predicted change in SA as degradation proceeds is quantified by calculating a normalised value with respect to that at initialisation, $SA^{\#}$. The simulations using Rubik configurations show a pattern of SA increase that is in marked contrast to that of an equivalent standard (non-Rubik) sphere of the type that is typically used in biogeochemical models. The Rubik simulations each show an increase in $SA^{\#}$ from its initial value as sub-units (volume) are removed from the matrix. This rate of increase in $SA^{\#}$ is greatest for the highest-resolution grids, here 2000×. SA remains above its initial value ($SA^{\#} > 1$) throughout much of the duration, eventually declining to zero when degradation is complete at which point no sub-units remain. Variability is seen between individual Rubik simulations for a given model configuration because sub-units are removed from the matrix based on random selection of exposed faces. This impact of stochasticity on modelled particle degradation is greatest for coarse resolution grids. The calculated $SA^{\#}$ of an equivalent standard (non-Rubik) sphere (the grey line in Fig. 2) decreases from the outset as it diminishes in size. Corresponding results for Rubik spheroids are shown in Supplementary Appendix 2.

Curve fits (black dashed lines in Fig. 2) were calculated using nonlinear regression for each GR based on averages of each of the 10-member ensembles:

$$SA^{\#}(GR, \varepsilon) = \left[k_1 + k_2\varepsilon + k_3\varepsilon^3 + k_4\left(0.5^{k_5\varepsilon}\right) \right] \qquad (1)$$
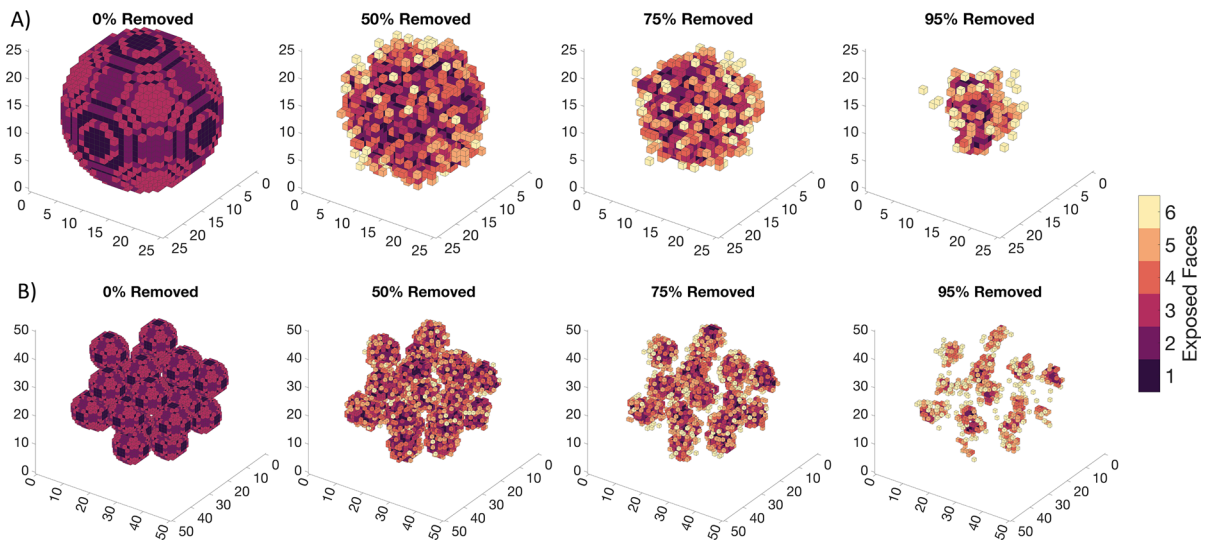
Fig. 1 Model simulations: **A** 25× Rubik particle, **B** 50× Rubik aggregate made up of 11× sub-particles. Snapshots show initial condition (0% sub-units removed) and 50, 75 and 95% sub-unit removal. Colouration indicates number of exposed faces of individual sub-units
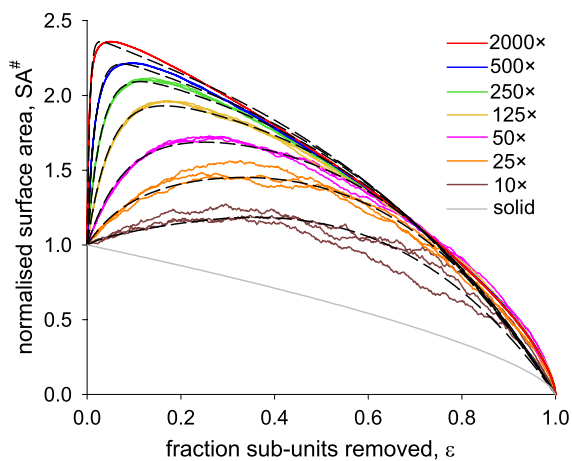
Fig. 2 Simulations (three shown for each configuration) showing normalised surface area ($SA^{\#}$) versus fraction sub-units removed (ε) for spheres at 10×GR (brown), 25×(orange), 50×(pink), 125×(gold), 250×(green), 500×(blue) and 2000×(red). Fitted curves (black dashed lines; Eq. 1) are based on 10-simulation ensemble averages. The grey line is for a standard (non-Rubik) sphere

where ε is the fraction of sub-units removed. Solutions were forced through the points (0, 1) and (1, 0), as required by the microbial model (below) and so only three of the parameters are free. Values for the coefficients, k_1–k_5, are listed in Supplementary Appendix 3.
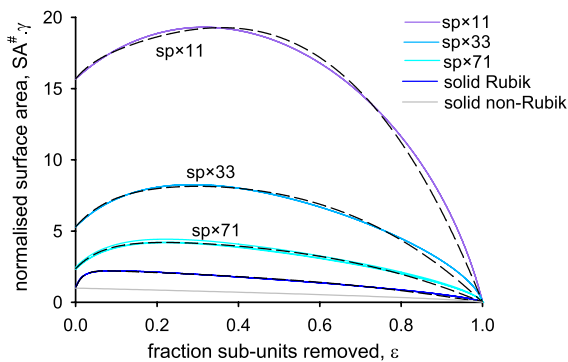
Aggregate particles

The Rubik particles examined above were initialised as a solid matrix of sub-units whereas many ocean particles, e.g., aggregates, are highly porous. In order to further increase the realism in our approach, porosity (ϕ) is now introduced by generating detritus particles that are constructed as aggregates of sub-particles which are themselves Rubik spheres (Fig. 1B). For example, an aggregate particle with GR 500× is constructed as follows. A notional empty spherical container is first created with dimensions 500×500×500. Sub-particle size is specified on the same grid, e.g., sp×25 would mean that sub-particle diameter is 25 sub-units, i.e., 1/20 that of the aggregate as a whole. A single sub-particle is first placed at the geometric centre of the container. Additional sub-particles are then added to the aggregate by bringing them in randomly from all directions in x, y and z ensuring that each new addition, which fuses on encounter, does not exceed the container boundary and that the sub-particle does not overlap any existing sub-particles at the contact point (it is discarded in either instance). The aggregate is built up until, as far as possible, the container is filled (for additional details, see Supplementary Appendix 7). Porosity is generated as gaps appear between sub-particles

during the packing process and it is quantified relative to an equivalent non-porous Rubik particle that has a default porosity of zero. Note that an aggregate is not the same as the requisite number of sub-particles in isolation to each other because sub-particles are conjoined to each other via shared sub-unit faces.

Here, we consider aggregates of 500×GR that are made up of sub-particles that are either sp×11 (11 sub-units), sp×33 or sp×71 in diameter. Based on 10-member ensembles, the aggregates contained 32,870 (invariant), 1217 (invariant) and 117.3 (average; range 112–122) sub-particles for sp×11, sp×33 and sp×71, respectively, with resulting average calculated porosities of 0.63, 0.65 and 0.66. Predicted trends in SA versus sub-unit removal are shown for these aggregate particles in Fig. 3, comparing with those of a solid Rubik and a solid (non-Rubik) sphere (as shown in Fig. 2).

The SA of aggregate particles at initialisation is greater than that of a solid (non-porous) particle of equivalent diameter because of the porosity introduced during aggregate formation. We quantify the relative increase as γ [GR, sp×] which is determined empirically by running the model for different grid resolutions and sub-particle sizes. In order to show this increase at initialisation, normalised SA (the y-axis in Fig. 3) is plotted as the product of $SA^{\#}$ and γ, noting that γ = 1.0 for non-aggregate Rubik particles. Metric γ can vary slightly for different

Fig. 3 Simulations (three for each configuration) showing normalised SA ($SA^{\#}$ multiplied by γ) versus fraction sub-units removed (ε) for **A** a solid 500×Rubik sphere (blue, as in Fig. 2) and **B** 500×Rubik aggregates made up of sub-particles with diameters of 11 (purple), 33 (pale blue) and 71 (cyan) sub-units. Fitted curves (black dashed lines) are shown (Eq. 1 multiplied by γ). The grey line is for a standard (non-Rubik) sphere

simulation runs because aggregate formation is a random process; average values based on 10-simulation ensembles, for each configuration, are provided in Supplementary Appendix 3. Results again demonstrate the characteristic increase in SA as each simulation progresses, before decreasing to zero when sub-unit removal is complete (Fig. 3). The trend becomes relatively flatter relative to initial condition, i.e., there is relatively less increase in normalised SA, as sub-particle size diminishes.

Microbial degradation

A simple model of microbial degradation is now presented that incorporates the SAMURAI results and represents the detritus biomass of individual particles, D (µmol C), generating time-dependent remineralisation rates that are directly comparable with those of traditional modelling approaches such as shrinking spheres. The changing SA of a particle as it degrades is calculated using the curve fits for $SA^{\#}$ described above (Eq. 1; Figs. 2, 3). Our default scenario is a spherical particle or aggregate with initial diameter, $d_{init} = 0.7$ mm, which is typical for phytoplankton aggregates (Iversen and Lampitt 2020), and density (filled, non-porous volume), $\omega = 40$ µmol C mm^{-3} ≈ 0.5 g C cm^{-3} which is typical of copepod faecal pellets (Honjo and Roman 1978) and phytoplankton cells (Persson et al. 2021). The initial SA (SA_{init}, mm^2), biomass volume (V_{init}, mm^3) and biomass of the particle, D_{init} (µmol C) are:

$$SA_{init} = 4\pi r_{init}^2 \gamma \qquad (2)$$

$$V_{init} = \frac{4}{3}\pi r_{init}^3 (1 - \varphi_{init}) \qquad (3)$$

$$D_{init} = \omega V_{init} \qquad (4)$$

where r_{init} is particle radius = $d_{init}/2$ and ϕ_{init} is initial porosity. For a non-aggregate particle ($\phi_{init} = 0$, γ = 1), and with parameter settings as described above, D_{init} is 7.2 µmol C. The SA (mm^2) of the Rubik sphere at any time t in the simulation, SA_t, is determined as the product of SA_{init} and $SA^{\#}$:

$$SA_t = SA_{init} SA^{\#}(GR, spx, \varepsilon_t) \qquad (5)$$

where the cumulative amount of detritus remineralised at time t is specified as a fraction of D_{init}, ε_t:

$$\varepsilon_t = 1 - \frac{D_t}{D_{init}} \tag{6}$$

A key model assumption is that microbial degradation of detritus biomass is proportional to the available SA that microbes act on, mediated by a rate constant, m_D (μmol C mm^{-2} d^{-1}):

$$\frac{dD}{dt} = -m_D SA_t \tag{7}$$

We now simulate the degradation of 0.7 mm Rubik particles. Default values for m_D and GR are required. Starting with the latter, we selected a default GR of 500× which, for a 0.7 mm particle, equates to a subunit diameter of 1.4 μm that corresponds approximately to the size of a typical marine bacterium (Lee and Fuhrman 1987; Børsheim et al. 1990), thereby assuming that ectoenzyme release produces patchiness on this scale. The resulting diameters of sub-particles at 11×, 33× and 71× (as in Fig. 3) are 15, 45 and 100 μm, respectively, which are typical of many nano- and microphytoplankton cells in the ocean (Sieburth et al. 1978; Brotas et al. 2022). A typical biomass-specific detritus remineralisation rate is 0.054 d^{-1} for marine aggregates (Bach et al. 2019 and references therein). Based on this value, we use $m_D = 0.0166$ μmol C mm^{-2} d^{-1} which is the rate predicted at the onset of a simulation for a 500× aggregate made up of 45 μm sub-particles (sp×33).

The predicted degradation of a 500× Rubik sphere over 100 days is compared with equivalent simulations using GRs of 50×, 125× and 2000×, along with simulations for 500× aggregate particles made up of sub-particles of either 100 μm (sp×71), 45 μm (sp×33) or 15 μm diameter (sp×11) (Fig. 4). Predicted degradation rates of the standard (non-aggregate) Rubik particles are similar across this range of GRs (Fig. 4A); the time taken for 90% degradation to occur varies between 204 days at 50×, 187 days at 500× and 185 days at 2000× GR. In contrast, the predicted loss rate of an equivalent non-Rubik sphere is approximately half, leading to a 90% degradation duration of 452 days. Predicted degradation is as much as two orders of magnitude faster for the aggregate particles. Whereas the average biomass-specific rate over the first 10 days is 0.0066 d^{-1} for

the standard 500× Rubik, the corresponding rates for Rubik aggregates are 0.050, 0.124 and 0.461 d^{-1} for sp×71, sp×33 and sp×11, respectively, with 90% degradation durations of 28, 14 and 6 days. Again, predicted degradation rate for equivalent non-Rubik aggregates are approximately half, with 90% degradation durations of 64, 30 and 10 days for sp×71, sp×33 and sp×11.

Surface area follows the trends of SA$^{\#}$ (Fig. 2) and is highly dynamic in all the Rubik simulations, in contrast to the progressive decline seen in the non-Rubik particles (Fig. 4B). Degradation is proportional to SA (Eq. 7) and thus predicted degradation rates are also highly dynamic over time (even more so when converted to biomass-specific rates: see Supplementary Appendix 4), as well as varying between the different model configurations. In case of the 500× (non-aggregate) and 500× sp11 (aggregate) simulations, for example, whereas average rates over the first 10 days are 0.066 and 0.46 d^{-1}, the corresponding ranges are 0.0036–0.0084 and 0.15–0.68 d^{-1} for the two configurations, respectively.

The size of detritus particles in the ocean varies considerably, e.g., a typical range for aggregates is between 0.04 and 2.98 mm in diameter in the North Atlantic (Iversen and Lampitt 2020). In general, smaller particles are expected to degrade fastest, at least in the case of non-porous particles, because of their greater surface area to volume ratios. The model does indeed reproduce this trend—predictions for Rubik particles with initial diameters of 0.35, 0.7, 1.4 and 2.8 mm are shown in Supplementary Appendix 5, noting that sub-unit size within the matrix is maintained by using GRs of 250×, 500× (our standard configuration), 1000× and 2000×.

Discussion

Using a new model, SAMURAI_1.0, we challenge the fundamental concept that surface area (SA) decreases as particles diminish in size during degradation by proposing the opposite, i.e., that the SA of detrital particles increases as they degrade due to the generation of microscale structure via microbial ectoenzymatic attack. Our study provides strong support for this idea: the simulated SA of individual detrital particles increased significantly in the early stages of degradation as microstructure proliferates,
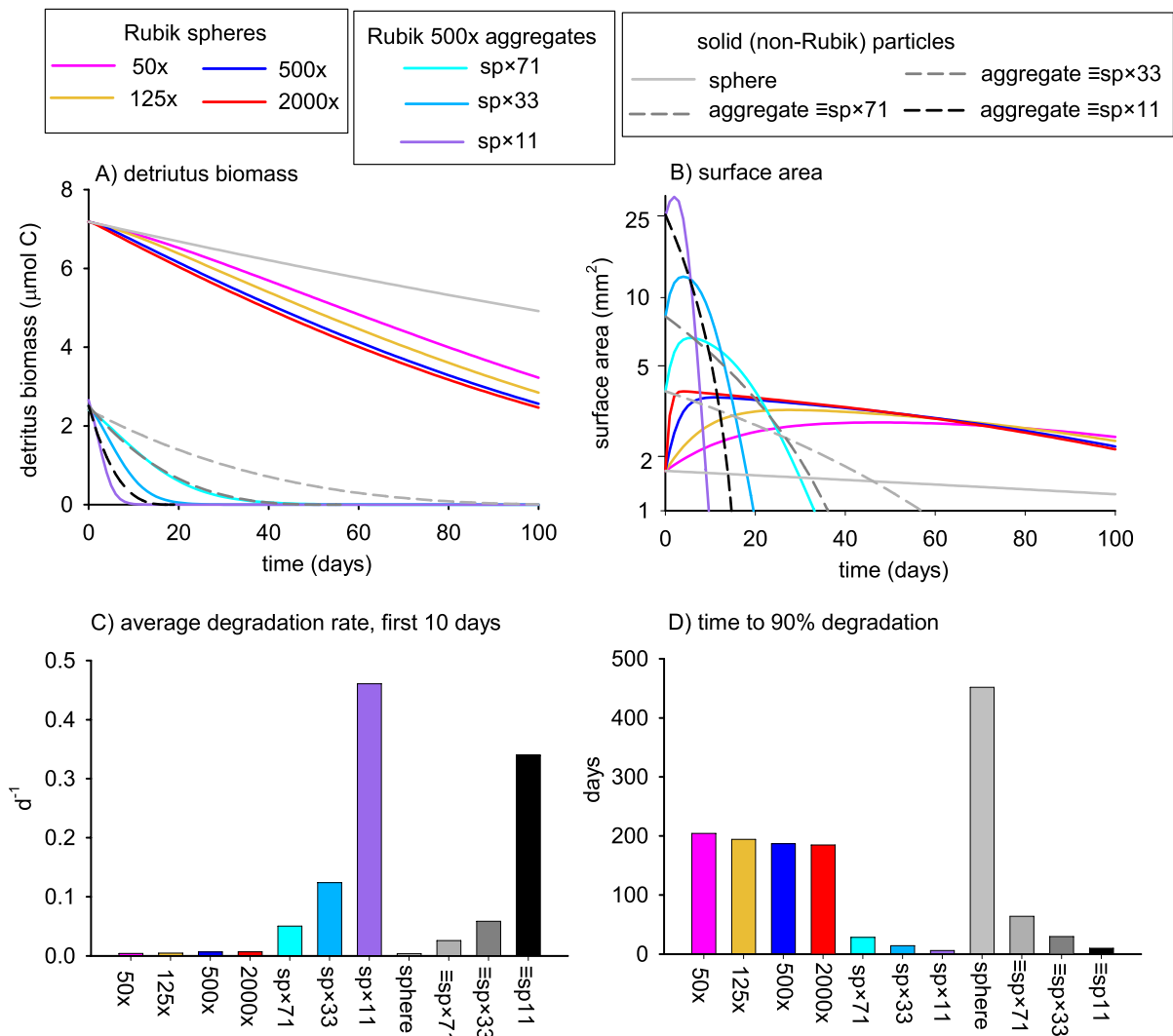
Fig. 4 100-day simulations for 0.7 mm diameter particles: standard (non-porous) Rubik spheres at grid resolutions 50×, 125×, 500× and 2000×, Rubik aggregates (×500) made up of sub-particles with diameters of 71× (100 μm), 33× (45 μm) and 11× sub-units (15 μm), and equivalent (≡) non-Rubik solid spheres and aggregates. **A** detritus biomass (μmol C), **B** surface area (mm²), **C** average biomass-specific degradation rate over the first 10 days (d⁻¹), **D** time taken to 90% degradation

in marked contrast to the decreasing SA predicted for shrinking spheres of the kind commonly used to represent particles in ocean biogeochemical models (e.g., Bianchi et al. 2018; Alcolombri et al. 2021; Nguyen et al. 2022). As a consequence, predicted remineralisation rates were approximately double those of conventional approaches. Faster remineralisation of sinking particulate organic matter means that the associated C will be released at shallower depths in the water column than otherwise predicted, lessening the potential for C sequestration in the deep ocean

interior via the biological gravitational pump. Our results suggest that SA and particle remineralisation are highly dynamic, as well as highlighting variability associated with particle structure, notably porosity. For example, detrital aggregates are generally highly porous in comparison to other particles such as zooplankton faecal pellets (Ploug et al. 2008) and may as a consequence be remineralised much faster. These sources of variability should be factored into future studies of remineralisation length scales for ocean detritus and how these vary spatially and temporally

throughout the global ocean, noting that there is currently great uncertainty in this field of research (Marsay et al. 2015; Buesseler et al. 2020; Henson et al. 2022). Our work highlights the importance of achieving mechanistic understanding of the remineralisation process and the need for sophisticated representation and parameterisation of it in global biogeochemical models.

Model results suggest that rugosity should be a common feature of detrital particles in the ocean (Fig. 5). While this may arise during particle formation, we propose that rugosity will also be created by the action of microbes acting on the detrital substrate. The SAMURAI model promulgates this idea, employing a unique representation of particle structure as a matrix of sub-units that are progressively removed based on faces that are exposed to the external environment. Although this structure is an abstract representation of real detritus particles in the ocean, we contend that the sequential removal of sub-units from a 3D matrix is a conceptually consistent representation of how particle biomass and SA change during degradation. Ectoenzymes act heterogeneously on particle surfaces, reflecting the heterogenous distribution of microbes (Abell and Bowman 2005; Bižić-Ionescu et al. 2018; Zhang et al. 2018). At a more fundamental level, the process of enzymatic degradation can be thought of as the cleaving of monomers one by one from long chain polymers such as chitin or cellulose (Pérez et al. 2002; Beier and Bertilsson 2013), creating heterogeneity in structure
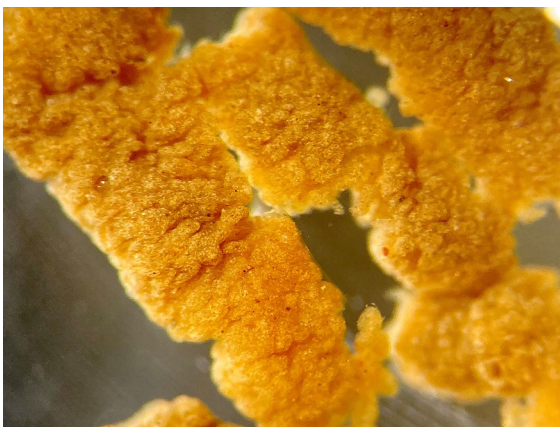
Fig. 5 Detrital aggregates produced by jellyfish from the subtropical South Atlantic, March 2023. Approximate width of pellets is 1.5 mm. Image: Mayor (2023)

at the molecular scale. A good analogy is the creation of microscale structure by acid etching on previously smooth glass or metal surfaces, in contrast to conventional models that represent particles as diminishing spheres which are akin to the shrinking of lollipops as they are sucked by children. We anticipate that our work will encourage new empirical studies to further investigate the nature and dynamics of particle SA and associated rugosity.

In order to incorporate SAMURAI within biogeochemical models, time-dependency was introduced using a fixed rate of remineralisation per unit exposed SA. This assumption is key to our approach and is justified on the basis that particles are typically densely covered by microbes (Simon et al. 2002) due to rapid colonisation by pelagic (free-living in the water column) bacteria (Kiørboe et al. 2003), meaning that carrying capacity is reached quickly. Rapid colonisation occurs for several reasons (Kiørboe et al. 2002): a significant fraction of pelagic bacteria are motile (Fenchel 2001; Grossart et al. 2001), water flowing over and through particles facilitates microbe-particle encounters (Ploug et al. 2002), and because bacteria are attracted to particles by chemosensory cues (Blackburn et al. 1998; Stocker and Seymour 2012).

We used a grid resolution (GR) of 500× as our standard Rubik configuration. For a typical particle of diameter 0.7 mm (Iversen and Lampitt 2020), this GR corresponds to a sub-unit diameter of 1.4 μm which is approximately the same size as a marine bacterium (Lee and Fuhrman 1987; Børsheim et al. 1990). This choice of GR is, we suggest, a reasonable starting assumption. In fact, the chosen GR turns out not to be particularly important because predicted degradation rates are similar for GRs between 50× and 2000×, while contrasting strongly (being much higher) than those of an equivalent non-Rubik detrital particle (Fig. 4). As well as Rubik spheres, other particle shapes can also be simulated using SAMURAI, e.g., we also generated results for particles represented as Rubik spheroids (Supplementary Appendix 2). These various shapes are generally representative of real ocean detritus which exists in many forms and sizes including aggregates and zooplankton faecal pellets (Durkin et al. 2021). Regarding size, we simulated the degradation of particles between 0.7 and 2.8 mm diameter (a typical range: Iversen and Lampitt 2020), maintaining sub-unit size at 1.4 μm which thereby required the use of GRs of 250×, 500×, 1000× and

2000× to simulate particles with diameters of 0.35, 0.7, 1.4 and 2.8 mm, respectively. As expected, predicted biomass-specific remineralisation rates showed an inverse relationship with size because smallest particles have the greatest SA:volume ratios (Supplementary Appendix 5).

Many detrital particles in the ocean are present as aggregates of smaller particles, e.g., "marine snow" (Alldredge and Silver 1988). A characteristic feature of aggregates is that they are porous, providing a large surface area for microbes to act on (Lampitt et al. 1993; Maerz et al. 2020). We introduced porosity into our analysis by setting up and investigating the degradation of aggregate particles in SAMU-RAI, maintaining a total diameter of 0.7 mm and using spherical sub-particles of 100, 45 and 15 μm; a grid of 1.4 μm sub-units was used in each case, such that the corresponding sub-particle GRs were 71×, 33× and 11×, respectively. The resulting porosities were 0.66, 0.65 and 0.63, significantly higher than a theoretical minimum of 0.26 for dense packing spherical objects such as oranges and cannonballs (Hales 2000), but noting that porosity may commonly exceed 0.9 in ocean aggregates (Alldredge 1998). As for the standard Rubik particles, predicted rates of C remineralisation of the Rubik aggregates are about double those of equivalent non-Rubik particles. The high porosity of the Rubik aggregates means that they degrade an order of magnitude faster than a non-porous Rubik sphere of the same size. Thus, rugosity aside, our results demonstrate the importance of particle structure, porosity, and associated variability in SA in particle remineralisation in the ocean.

The degradation of detritus in ocean biogeochemical models is typically modelled using a fixed or temperature-dependent rate per unit biomass (Yool et al. 2013; Aumont et al. 2015; Kriest and Oschlies 2015). Our Rubik model assumes instead that degradation is proportional to SA. This assumption is, we suggest, more realistic because microbial ectoenzymes act on particle surfaces (Enke et al. 2018) and leads to profoundly different results from other models because biomass-specific degradation rate varies over time with changing SA:biomass (SA:volume) ratio. Rates may likewise vary between particles with different porosities such as zooplankton faecal pellets and phytoplankton aggregates. The use of SA as a descriptor necessarily entails the representation of detritus as individual particles, along with associated variation

in shape and porosity, because one must resolve particles' SA and not just their mass. Assigning a value for the degradation rate parameter also poses a significant challenge. We used $m_D = 0.0166$ μmol C mm^{-2} d^{-1} which, using a density of 0.5 g C cm^{-3}, corresponds to a biomass-specific rate of 0.054 d^{-1} for a typical Rubik aggregate particle (in its initial state before any degradation occurs) that matches an empirical estimate derived from observations of marine aggregates (Bach et al. 2019 and references therein). It is therefore unsurprising that our predicted degradation times of aggregate particles using SAMURAI are realistic: 0.7 mm Rubik aggregates made up sub-particles of 15, 45 or 100 μm, took 6, 14 and 28 days to reach 90% degradation, respectively (Fig. 4D). In contrast, the corresponding 90% degradation time for a standard (solid, non-aggregate) Rubik particle of 0.7 mm diameter was 187 days which is well beyond typical timescales of up to a few weeks (e.g. Boyd et al. 1999; Schmidt et al. 2002; Omand et al. 2020; Nguyen et al. 2022). This mismatch could be addressed by increasing the degradation rate, e.g., by an order of magnitude to $m_D = 0.166$ μmol C mm^{-2} d^{-1}. The 0.7 mm standard particle then reaches 90% turnover ten times faster in a realistic timescale of 18.7 days because degradation timescale scales linearly with parameter m_D. In contrast, however, the aggregate particle now reaches this milestone in little over half a day which is unrealistically too fast. The hypothetical particle shapes that we examined here, i.e., solid spherical particles and aggregates made up of sub-particles, while providing an excellent theoretical examination of the new Rubik approach, are idealised in form. For example, the assumption of zero porosity in the non-aggregate Rubik particles is clearly a simplification as even relatively dense particles such as faecal pellets can have a porosity of 0.65 (Ploug et al. 2008). Deriving a universal parameterisation in which degradation timescales are accurately predicted for a range of particle types, using a single value of m_D, will require future model development to represent different particle types with greater realism, facilitated by improved observations to quantify particle characteristics—shape, biomass, SA, volume and porosity—and how they change through time. Likewise, new measurements of degradation rates for a range of particle types are needed in order to realistically parameterise detritus remineralisation in biogeochemical models.

There are some interesting theoretical considerations associated with the Rubik modelling approach. The evolution of particle SA using SAMURAI, and thereby differences associated with GR, can be understood in terms of the way that sub-units within the Rubik matrix are progressively removed. The probability of any one sub-unit within the grid being selected at a given point in the sequence is proportional to its number of exposed faces. This selection procedure means that sub-units in the outermost layers of the matrix have the highest likelihood of being removed because they tend to have many exposed faces (Fig. 1). Sub-units deeper within the matrix can also be removed but, because they tend to have few exposed faces the probability of them being removed is lower. The generation of burrows or tunnels, while possible, is therefore less likely. Use of a high GR, i.e., a fine grid size, means that when inner layers are exposed, the resulting tunnels are relatively narrow and the associated newly exposed SA constitutes a smaller proportion of the Rubik total, relative to the corresponding case for coarser grids. As a consequence, removal of sub-units from the outer layers is more likely such that SA proliferates most rapidly and achieves higher maximum values at high GRs (Fig. 2). This maximum will ultimately saturate as GR is increased towards an infinite number of sub-units within the matrix (additional information on convergence is provided in Supplementary Appendix 6).

The increase in rugosity and associated SA driven by microbial action will theoretically become less important when simulating highly porous detrital aggregates. For example, in the case of our 0.7 mm Rubik aggregate made up of the smallest sub-particles, 15 μm, the predicted time to complete 90% degradation was 6.0 days, with a corresponding time of 10.0 days for an equivalent non-Rubik particle, a ratio of 0.6. The times for non-porous particles were 187 and 452 days, a ratio of 0.41. High initial porosity means that the increase in SA[#] in the early stages of degradation is relatively less for highly porous particles (Fig. 3). The extreme case is a lattice in which sub-units are connected only at their corners. SA is maximal and will decrease from the outset as sub-units are removed from the matrix.

The representation of biology in SAMURAI is basic but nevertheless sufficient to highlight the importance of representing the evolution of particle SA when modelling the degradation of sinking detritus in the ocean, and the complexities thereof. A number of avenues could be pursued to further improve the realism of the SAMURAI model. We assumed that removal of sub-units from the matrix is random based on faces exposed (in contact with) the external environment. There will in reality be a declining oxygen gradient towards the particle interior (Alldredge and Cohen 1987; Ploug et al. 2008) such that biomass associated with internal SA will degrade more slowly. Future work could simulate the influence of this gradient on particle degradation in SAMURAI, requiring hydrodynamic modelling of the associated fluid dynamics in the surrounding water. All sub-units within the Rubik matrix are treated as the same, whereas in reality detritus particles in the ocean exhibit variability in particle structure, biochemical makeup and microbial community composition. Bacteria have a range of affinities for various substrates which are degraded at different rates, with the most labile being used first (Grossart and Ploug 2000, 2001). To complicate matters, some substrates may be physically protected by the presence of minerals (Rothman and Forney 2007). A future version of SAMURAI could include a matrix where sub-units are assigned different labilities. Dealing with microbial diversity on marine particles is an even more complex issue, not least because of species succession in the resident community (Datta et al. 2016; Pelve et al. 2017) will likely drive differences in resource requirements. Our understanding of microbial succession on sinking particles, and the consequences for ocean biogeochemistry, remains in its infancy. Nevertheless, SAMURAI provides an excellent candidate model for quantifying the effects of microbial community interactions as understanding of these matures. Finally, representation of particle structure merits further attention. A general feature of marine aggregates is that packing density decreases with increasing particle size, giving rise to a fractal dimensional < 3 (Logan and Wilkinson 1990; Jackson 1995). The packing process used to generate our Rubik aggregates, random encounter, leads to a fractal dimension ≈ 3, meaning that packing density does not decrease with particle size. The SAMURAI model can handle any particle structure that is input as sub-unit presence/absence on an x–y–z grid, providing plenty of opportunity for future research.

We have demonstrated that simulating particle degradation via sub-unit removal from a Rubik matrix yields results that are in marked contrast to those derived from simulations of shrinking spheres, with important consequences for ocean C sequestration. The model presented here suggests the need for a reappraisal of current methods for representing particle degradation in ocean models. Further studies, including observations of the surface characteristics of real detritus particles and of microbial dynamics and enzymatic degradation of organic matter, are required to consolidate our findings.

Conclusion

The degradation of sinking detritus in the ocean is typically modelled by assuming that particles behave as shrinking spheres, the surface area (SA) of which declines progressively as they are degraded. We challenge this concept by proposing that the action of microbial ectoenzymes serves to increase SA as particles degrade due to the generation and proliferation of microscale rugosity. Our study explores this concept using a new model, SAMURAI_1.0, which represents particles as a 3D matrix of sub-units, analogous to the infamous Rubik's Cube, where sub-unit removal represents decay of organic matter exposed to the external environment by microbial ectoenzymes. We show that the effect of increasing SA during the early stages of degradation could be highly significant, doubling predicted remineralisation rates. As a consequence of fast remineralisation rates, the C release accruing from the degradation of sinking particles, as predicted by ocean biogeochemical models, will occur at shallower depths than otherwise expected, with less sequestration of C in the ocean's interior. Predicted particle SA and remineralisation are highly dynamic and sensitive to porosity in SAMURAI, necessitating careful representation in biogeochemical models. We suggest that our Rubik-inspired approach represents a significant advance in conceptualising and parameterising detritus particles in ocean models. Our work highlights the need for further studies, both observational and modelling, to corroborate our ideas by examining remineralisation in detritus particles and the associated dynamics of SA. New understanding will lead to improved parameterisations of organic matter remineralisation and C sequestration in global

biogeochemical models and, in turn, this will reduce uncertainty in projections of the future response of the ocean's biological gravitational pump and its role in global climate regulation.

Data availability   The SAMURAI_1.0 model is available as a Windows app, coded in C++. It, along with accompanying user manual and source code, can be downloaded at the GitHub online repository: https://github.com/gitbeast7/Samurai (the user manual is also shown in Supplementary Appendix 7).

Declarations

Conflict of interest   The authors declare that they have no conflict of interest.

References

Abell GCJ, Bowman JP (2005) Colonization and community dynamics of class *Flavobacteria* on diatom detritus in experimental mesocosms based on Southern Ocean seawater. FEMS Microb Ecol 53:379–391. https://doi.org/10.1016/j.femsec.2005.01.008

Alcolombri U, Peaudecerf FJ, Fernandez VI, Behrendt L, Lee KS, Stocker R (2021) Sinking enhances the degradation of organic particles by marine bacteria. Nature GeoSci 14:775–780. https://doi.org/10.1038/s41561-021-00817-x

Alldredge A (1998) The carbon, nitrogen and mass content of marine snow as a function of aggregate size. Deep Sea Res I 45:529–541. https://doi.org/10.1016/S0967-0637(97)00048-4

Alldredge AL, Cohen Y (1987) Can microscale chemical patches persist in the sea? Microelectrode study of marine snow, fecal pellets. Science 235:689–691. https://doi.org/10.1126/science.235.4789.689

Alldredge AL, Silver MW (1988) Characteristics, dynamics and significance of marine snow. Prog Oceanogr 20:41–82. https://doi.org/10.1016/0079-6611(88)90053-5

Arnosti C (2011) Microbial extracellular enzymes and the marine carbon cycle. Annu Rev Mar Sci 3:401–425. https://doi.org/10.1146/annurev-marine-120709-142731

Aumont O, Ethé C, Tagliabue A, Bopp L, Gehlen M (2015) PISCES-v2: an ocean biogeochemical model for carbon and ecosystem studies. Geosci Model Dev 8:2465–2513. https://doi.org/10.5194/gmd-8-2465-2015

Bach LT, Stange P, Taucher J, Achterberg EP, Algueró-Muñiz M, Horn H, Esposito M, Riebesell U (2019) The influence of plankton community structure on sinking velocity and remineralization rate of marine aggregates. Global Biogeocem Cycles 33:971–994. https://doi.org/10.1029/2019GB006256

Beier S, Bertillson S (2013) Bacterial chitin degradation—mechanisms and ecophysiological strategies. Front Microbiol 4:149. https://doi.org/10.3389/fmicb.2013.00149

Bianchi D, Weber TS, Kiko R, Deutsch C (2018) Global niche of marine anaerobic metabolisms expanded by particle microenvironments. Nature Geosci 11:263–268. https://doi.org/10.1038/s41561-018-0081-0

Bižić-Ionescu M, Ionescu D, Grossart H-P (2018) Organic particles: heterogeneous hubs for microbial interactions in aquatic ecosystems. Front Microbiol 9:2569. https://doi.org/10.3389/fmicb.2018.02569

Blackburn N, Fenchel T, Mitchell J (1998) Microscale nutrient patches in planktonic habitats shown by chemotactic bacteria. Science 282:2254–2256. https://doi.org/10.1126/science.282.5397.2254

Børsheim KY, Bratbak G, Heldal M (1990) Enumeration and biomass estimation of planktonic bacteria and viruses by transmission electron microscopy. Appl Environm Microbiol 56:352–356. https://doi.org/10.1128/aem.56.2.352-356.1990

Boyd PW, Sherry ND, Berges JA, Bishop JKB, Calvert SE, Charette MA, Giovannoni SJ, Goldblatt R, Harrison PJ, Moran SB, Roy S, Soon M, Strom S, Thibault D, Vergin KL, Whitney FA, Wong CS (1999) Transformations of biogenic particulates from the pelagic to the deep ocean realm. Deep Sea Res II 46:2761–2792. https://doi.org/10.1016/S0967-0645(99)00083-1

Boyd PW, Claustre H, Levy M, Siegel DA, Weber T (2019) Multifaceted particle pumps drive carbon sequestration in the ocean. Nature 568:327–335. https://doi.org/10.1038/s41586-019-1098-2

Brotas V, Tarran GA, Veloso V, Brewin RJW, Woodward EMS, Airs R, Beltran C, Ferreira A, Groom SB (2022) Complementary approaches to assess phytoplankton groups and size classes on a long transect in the Atlantic Ocean. Front Mar Sci 8:682621. https://doi.org/10.3389/fmars.2021.682621

Buesseler KO, Boyd PW, Black EE, Siegel DA (2020) Metrics that matter for assessing the ocean biological carbon pump. Proc Natl Acad Sci USA 117:9679–9687. https://doi.org/10.1073/pnas.1918114117

Chróst RJ (1992) Significance of bacterial ectoenzymes in aquatic environments. Hydrobiologia 243(244):61–70. https://doi.org/10.1007/BF00007020

Datta MS, Sliwerska E, Gore J, Polz MF, Cordero OX (2016) Microbial interactions lead to rapid micro-scale successions on model marine particles. Nat Commun 7:11965. https://doi.org/10.1038/ncomms11965

Demaine ED, Demaine ML, Eisenstat S, Lubiw A, Winslow A (2011) Algorithms for solving Rubik's Cubes. In: Demetrescu C, Halldórsson MM (eds) Algorithms—ESA 2011. Proceedings 19th annual European symposium Saarbrücken, Germany, September 5–9, 2011. Springer, Berlin, pp 689–700. https://doi.org/10.1007/978-3-642-23719-5

Durkin CA, Buesseler KO, Cetinić I, Estapa M, Kelly RP, Omand M (2021) A visual tour of carbon export by sinking particles. Global Biogeochem Cycles 35:e2021GB006985. https://doi.org/10.1029/2021GB006985

Enke TN, Leventhal GE, Metzger M, Saavedra JT, Cordero OX (2018) Microscale ecology regulates particulate organic matter turnover in model marine microbial communities. Nat Commun 9:2743. https://doi.org/10.1038/s41467-018-05159-8

Fenchel T (2001) Eppur si muove: many water column bacteria are motile. Aquat Microb Ecol 24:197–201. https://doi.org/10.3354/ame024197

Field CB, Behrenfeld MJ, Randerson JT, Falkowski P (1998) Primary production of the biosphere: integrating terrestrial and oceanic components. Science 281:237–240. https://doi.org/10.1126/science.281.5374.237

Grossart H-P, Ploug H (2000) Bacterial production and growth efficiencies: direct measurements on riverine aggregates. Limnol Oceanogr 45:436–445. https://doi.org/10.4319/lo.2000.45.2.0436

Grossart H-P, Ploug H (2001) Microbial degradation of organic carbon and nitrogen on diatom aggregates. Limnol Oceanogr 46:267–277. https://doi.org/10.4319/lo.2001.46.2.0267

Grossart H-P, Riemann L, Azam F (2001) Bacterial motility in the sea and its ecological implications. Aquat Microb Ecol 25:247–258. https://doi.org/10.3354/ame025247

Hales TC (2000) Cannonballs and honeycombs. Not Am Math Soc 47:440–449

Henson SA, Sanders R, Madsen E (2012) Global patterns in efficiency of particulate organic carbon export and transfer to the deep ocean. Glob Biogeochem Cycles 26:1028. https://doi.org/10.1029/2011GB004099

Henson SA, Laufkötter C, Leung S, Giering SLC, Palevsky HI, Cavan EL (2022) Uncertain response of ocean biological carbon export in a changing world. Nature Geosci 15:248–254. https://doi.org/10.1038/s41561-022-00927-0

Honjo S, Roman MR (1978) Marine copepod faecal pellets: production, preservation and sedimentation. J Mar Res 36:45–57

Iversen MH, Lampitt RS (2020) Size does not matter after all: no evidence for a size-sinking relationship for marine snow. Prog Oceanogr 189:102445. https://doi.org/10.1016/j.pocean.2020.102445

Jackson GA (1995) Comparing observed changes in particle size spectra with those predicted using coagulation theory. Deep Sea Res II 42:159–184. https://doi.org/10.1016/0967-0645(95)00010-N

Kiørboe T, Grossart H-P, Ploug H, Tang K (2002) Mechanisms and rates of bacterial colonization of sinking aggregates. Appl Environm Microbiol 68:3996–4006. https://doi.org/10.1128/AEM.68.8.3996-4006.2002

Kiørboe T, Tang K, Grossart H-P, Ploug H (2003) Dynamics of microbial communities on marine snow aggregates:

colonization, growth, detachment, and grazing mortality of attached bacteria. Appl Environm Microbiol 69:3036–3047. https://doi.org/10.1128/AEM.69.6.3036-3047.2003

Kriest I, Oschlies A (2015) MOPS-1.0: towards a model for the regulation of the global oceanic nitrogen budget by marine biogeochemical processes. Geosci Model Dev 8:2929–2957. https://doi.org/10.5194/gmd-8-2929-2015

Kwon EY, Primeau F, Sarmiento JL (2009) The impact of remineralization depth on the air–sea carbon balance. Nat Geosci 2:630–635. https://doi.org/10.1038/ngeo612

Lampitt RS, Wishner KF, Turley CM, Angel MV (1993) Marine snow studies in the Northeast Atlantic Ocean: distribution, composition and role as a food source for migrating plankton. Mar Biol 116:689–702. https://doi.org/10.1007/BF00355486

Lee S, Fuhrman JA (1987) Relationships between biovolume and biomass of naturally derived marine bacterioplankton. Appl Environm Microbiol 53:1298–1303. https://doi.org/10.1128/aem.53.6.1298-1303.1987

Logan BE, Wilkinson DB (1990) Fractal geometry of marine snow and other biological aggregates. Limnol Oceanogr 35:130–136. https://doi.org/10.4319/LO.1990.35.1.0130

Maerz J, Six KD, Stemmler I, Ahmerkamp S, Ilyina T (2020) Microstructure and composition of marine aggregates as co-determinants for vertical particulate organic carbon transfer in the global ocean. Biogeosciences 17:1765–1803. https://doi.org/10.5194/bg-17-1765-2020

Marsay CM, Sanders RJ, Henson SA, Pabortsava K, Achterberg EP, Lampitt RS (2015) Attenuation of sinking particulate organic carbon flux through the mesopelagic ocean. Proc Natl Acad Sci USA 112:1089–1094. https://doi.org/10.1073/pnas.1415311112

Mayor DJ (2023) Zooming in on the jellyfish faecal pellets (Instagram @oceanplankton). 09/03/2023. Retrieved from https://www.instagram.com/p/CpkS00ys9kd/. Accessed 16/05/2023

Nguyen TTH, Zakem EJ, Ebrahimi A, Schwartzman J, Caglar T, Amarnath K, Alcolombri U, Peaudecerf J, Hwa T, Stocker R, Cordero OX, Levine NM (2022) Microbes contribute to setting the ocean carbon flux by altering the fate of sinking particulates. Nat Commun 13:1657. https://doi.org/10.1038/s41467-022-29297-2

Omand MM, Govindarajan R, He J, Mahadevan A (2020) Sinking flux of particulate organic matter in the oceans: sensitivity to particle characteristics. Sci Rep 10:5582. https://doi.org/10.1038/s41598-020-60424-5

Pelve EA, Fontanez KM, DeLong EF (2017) Bacterial succession on sinking particles in the ocean's interior. Front Microbiol 8:2269. https://doi.org/10.3389/fmicb.2017.02269

Pérez J, Muñoz-Dorado J, de la Rubia T, Martínez J (2002) Biodegradation and biological treatments of cellulose, hemicellulose and lignin: an overview. Int Microbiol 5:53–63. https://doi.org/10.1007/s10123-002-0062-3

Persson A, Smith BC, Alix JH, Li Y, Holohan BA, Wikfors GH (2021) Differences in species mass density between dinoflagellate life stages and relevance to accumulation by hydrodynamic processes. J Phycol 57:1492–1503. https://doi.org/10.1111/jpy.13181

Ploug H, Hietanen S, Kuparinen J (2002) Diffusion and advection within and around sinking, porous diatom aggregates. Limnol Oceanogr 47:1129–1136. https://doi.org/10.4319/lo.2002.47.4.1129

Ploug H, Iversen MH, Fischer G (2008) Ballast, sinking velocity, and apparent diffusivity within marine snow and zooplankton fecal pellets: implications for substrate turnover by attached bacteria. Limnol Oceanogr 53:1878–1886. https://doi.org/10.4319/lo.2008.53.2.0469

Rothman DH, Forney DC (2007) Physical model for the decay and preservation of marine organic carbon. Science 316:1325–1328. https://doi.org/10.1126/science.1138211

Schmidt S, Chou L, Hall IR (2002) Particle residence times in surface waters over the north-western Iberian Margin: comparison of pre-upwelling and winter periods. J Mar Syst 32:3–11. https://doi.org/10.1016/S0924-7963(02)00027-1

Sieburth JMN, Smetacek V, Lenz J (1978) Pelagic ecosystem structure: heterotrophic compartments of the plankton and end their relationship to plankton size fractions. Limnol Oceanogr 23:1256–1263. https://doi.org/10.4319/lo.1978.23.6.1256

Simon M, Grossart H-P, Schweitzer B, Ploug H (2002) Microbial ecology of organic aggregates in aquatic ecosystems. Aquat Microb Ecol 28:175–211. https://doi.org/10.3354/ame028175

Smith DC, Simon M, Alldredge AL, Azam F (1992) Intensive hydrolytic activity on marine aggregates and implications for rapid particle dissolution. Nature 359:139–141. https://doi.org/10.1038/359139a0

Stocker R, Seymour JR (2012) Ecology and physics of bacterial chemotaxis in the ocean. Microb Molecular Biol Rev 76:792–812. https://doi.org/10.1128/MMBR.00029-12

Vetter YA, Deming JW, Jumars PA, Krieger-Brockett BB (1998) A predictive model of bacterial foraging by means of freely released extracellular enzymes. Microb Ecol 36:75–92. https://doi.org/10.1007/s002489900095

Wilson JD, Andrews O, Katavouta A, de Melo VF, Death RM, Adloff M, Baker CA, Blackledge B, Goldsworth FW, Kennedy-Asser AT, Liu Q, Sieradzan KR, Vosper E, Ying R (2022) The biological carbon pump in CMIP6 models: 21st century trends and uncertainties. Proc Natl Acad Sci USA 119:e2204369119. https://doi.org/10.1073/pnas.2204369119

Yool A, Popova EE, Anderson TR (2013) MEDUSA-2.0: an intermediate complexity biogeochemical model of the marine carbon cycle for climate change and ocean acidification studies. Geosci Model Dev 6:1767–1811. https://doi.org/10.5194/gmd-6-1767-2013

Zhang R, Liu B, Lau SCK, Ki J-S, Qian P-Y (2018) Particle-attached and free-living bacterial communities in a contrasting marine environment: Victoria Harbor, Hong Kong. FEMS Microbiol Ecol 61:496–508. https://doi.org/10.1111/j.1574-6941.2007.00353.x